Book of Tutorials and Abstracts

European Microbeam Analysis Society

EMAS 2023

17th

EUROPEAN WORKSHOP

on

MODERN DEVELOPMENTS AND APPLICATIONS IN MICROBEAM ANALYSIS

7 to 11 May 2023
at the
Jagiellonian University, Auditorium Maximum
Krakow, Poland

Under the auspices of the Rector of the
Jagiellonian University, Krakow, Poland
Organised in collaboration with the
Institute of Metallurgy and Materials Science of
the Polish Academy of Sciences, Krakow, Poland

EMAS
European Microbeam Analysis Society eV
www.microbeamanalysis.eu/

This volume is published by:
European Microbeam Analysis Society eV (EMAS)
EMAS Secretariat
c/o Eidgenössische Technische Hochschule, Institut für Geochemie und Petrologie
Clausiusstrasse 25
8092 Zürich
Switzerland

ISBN 978 90 8227 6961
NUR code: 972 – Materials Science

COUPLED SEM-EDS-RAMAN: A COMPLEMENTARY APPROACH FOR CHARACTERISATION - APPLICATION TO GEOMATERIALS

Guillaume Wille

B.R.G.M.
3 avenue Claude Guillemin , P.O Box 36009, 45060 Orléans Cedex 2, France
e-mail: g.wille@brgm.fr

Guillaume Wille graduated from the University of Orleans (France) with a PhD in Material Chemistry. He has worked as an electron microscopy engineer for private and public companies. Currently he is working as research scientist at BRGM (French Geological Survey) since 2007. He is in charge of an EPMA lab and an SEM coupled to Raman spectroscopy. He also works on various SEM and TEM. His current research topics focus on micro- and nano-characterisation applied to geomaterials, including asbestos in the natural environment, mining ore characterisation, and bio-mineral interface, ... He acts as a trainer on electron microscopy and microanalysis in various training courses. He authored or co-authored about 50 scientific papers and book chapters.
He has been a board member of the GN-MEBA (French Scanning Electron Microscopy and Microanalysis Group) since 2011.

1. INTRODUCTION

The combination of elemental and crystallographic analysis is frequently required to identify and describe natural and synthetic materials. Physical and chemical characterisation requires a set of analytical spectroscopic and/or imaging techniques to access a thorough knowledge of the sample, to better understand the structural, chemical, and textural factors that control their properties, their behaviour, and their reactivity, ... As an example, a mineral description often requires chemical information (major, minor, and trace elements), structural information (crystal structure, crystallinity…), and morphological information (crystal shape and size).

Among these techniques, scanning electron microscopy (SEM) and Raman spectroscopy occupy a major place among the characterization techniques and have often been combined in many studies. SEM provides various information on morphology, topography, and chemistry at a nanometre scale, supplemented by electron beam-based techniques providing chemical or crystallographic information, like energy- or wavelength-dispersive X-ray spectrometry (EDS, WDS), or electron backscatter diffraction (EBSD). Micro-Raman spectroscopy is also widely used in the organic or inorganic materials characterisation at a micrometre / sub-micrometre scale. The spectrum is unique for a given compound. It can provide details on the chemical and structural properties (functional groups, lattice defects, crystallinity, etc.). Raman offers various information, which includes, among others, the identification of polymorphs, crystallographic orientation, evaluation of temperature, and stress effects on the structure. Then, both are often used in parallel.

Switching from one to the other is in some cases considered a problem (relocation, identification). Coupling SEM-EDS and confocal Raman imaging on the same analytical system is an efficient method for the advanced physicochemical characterisation of materials and the determination of structural properties of materials at the micro-/sub-micrometre scale. The interest of the coupling will be illustrated by various examples of application to geomaterials and mineralogy, including cultural heritage materials, and naturally occurring asbestos, for which this coupling makes it possible to solve problems for characterisation.

2. COUPLING SEM-EDS AND RAMAN SPECTROSCOPY

2.1. Why coupling SEM and Raman spectroscopy

2.1.1. Background and principle of μ-Raman spectroscopy. In 1922, Brillouin [1] and Smekal [2] introduced the theoretical principle of inelastic scattering of light, experimentally demonstrated in 1928 by Raman and Krishnan [3]. However, despite numerous studies on this phenomenon, the so-called Raman effect did not succeed in becoming a useful technique for material characterisation. This was due to several technical constraints. During the 1960s, the development of laser sources and the μ-Raman systems, i.e., an optical

microscope equipped with a Raman spectrometer allowed new capacities for spectroscopy. With the development of CCDs, spectrometers and optical assembly, performance, and sensitivity have been improved. It then becomes a major and powerful analytical technique. Raman spectroscopy has developed into an effective tool for analysing natural and synthetic materials. It is widely recognised as a powerful tool for acquiring information about molecular vibrations, which provide details of the molecular specificity, structural features, and relatively simple spectral fingerprints of the material.

The Raman effect is related to the interactions between light and matter (Fig. 1). When photons interact with matter, then 1) part of the light is reflected; 2) part of the light is transmitted; 3) part of the light is absorbed; 4) part of the light is diffused. The diffusion is split into two contributions. A large part of the light keeps its energy, i.e., no energy is exchanged between photons and matter. This is called elastic scattering, or Rayleigh scattering [4] (about 0.1 % of the incident light). About 0.0001 % of the light is scattered with a change in energy, i.e., inelastic scattering also called Raman scattering [3]. The change in wavelength is measured relative to the incident wavelength and termed "Raman shift" (expressed in wavenumbers, cm^{-1}). The Raman shift is associated with two different energy bands. The shift at wavelengths higher than that of the incident light (lower wavenumber) is termed Stokes scattering. The shift at wavelengths lower than that of the incident light (higher wavenumber) is termed anti-Stokes scattering (Fig. 2). Typically, higher-intensity Stokes scattering peaks are used for analysis, but anti-Stokes peaks can also be used.

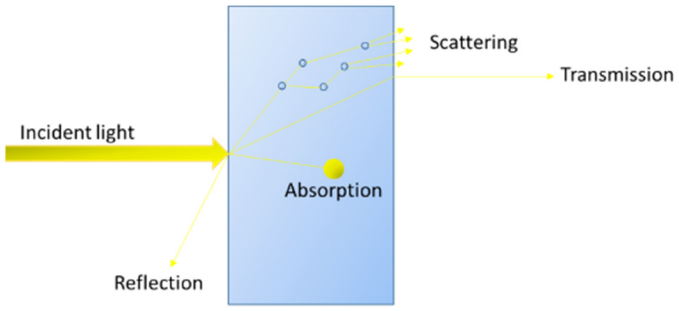

Figure 1. Schematic diagram of light / matter interactions.

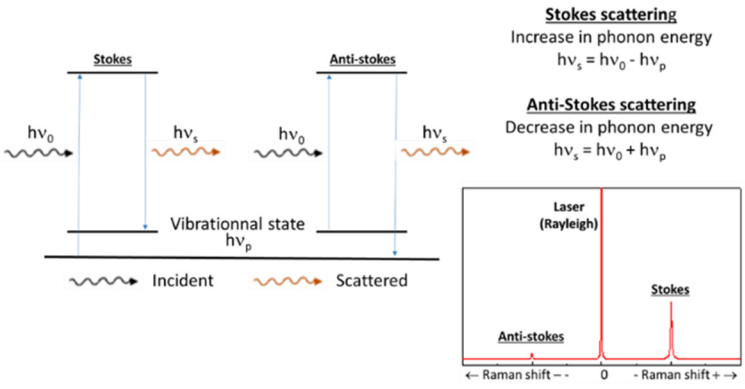

Figure 2. Stokes / anti-Stokes scattering.

The Raman shift is related to the vibrational energy levels in the ground electronic state of the molecule, and as such, the observed Raman shifts are a direct measure of the vibrational energies of the molecule. A Raman spectrum features several peaks, showing the several wavelength positions of the Raman scattered light. Each peak corresponds to a specific molecular bond vibration, including individual bonds and groups of bonds (C-C, aromatic ring, $–CO_3$, –OH, lattice modes, etc., …). Raman, therefore, provides a characteristic signature of the analysed phase.

2.1.2. Application of Raman spectroscopy. Raman spectroscopy is used in varied fields as a non-destructive, microscopic, chemical analysis and imaging technique. Raman analysis can provide key information to characterise the chemical composition and structure of a sample, whether solid, liquid, or gas. It is for example employed to analyse various characteristics and properties of the material: composition, purity [5-7], intrinsic stress/strain [8-10], structure and thickness of 2D materials layers [11-14], identification and characterisation of the typical features of ancient paints and pigments, precious stones, degradation of materials of cultural significance [15-18], etc. In geosciences, Raman applications are countless, for example, identification and distribution of minerals and polymorphs (same chemistry, different crystal structure) [19-21], fluid inclusions in minerals [22, 23], geothermometry [24], etc. Raman spectroscopy is a powerful analytical tool in geology and mineralogy, with advantages over alternative techniques: little or no sample preparation, microscopic technique complements conventional petrographic analysis, unambiguous mineral identification, a large variety of samples types (petrographic thin sections, polished samples, powders, piece of rock as it is, …). As Raman spectroscopy uses light, if a mineral is transparent to the laser wavelength, it is possible to analyse under the surface or acquire a stack of spectra/images. However, Raman spectroscopy is concerned with limitations. Not all compounds are Raman active (i.e., produce Raman peaks), or scattering efficiencies can be low for some phases. Raman spectroscopy cannot be used for some materials such as metals and alloys, or NaCl. The Raman effect is very weak and detection requires sensitive and highly optimised instrumentation. The Raman spectrum can be swamped by fluorescence (due to impurities or the sample itself) from some materials (although this can partly be solved by changing the laser wavelength). The beam energy can destroy or modify the sample. The resolution of an optical microscope in μ-Raman spectroscopy is limited by light diffraction and depth resolution can vary from one sample to another, due to the optical transmittance of each material.

2.1.3. From SEM-EDS and Raman to Raman in SEM. The interest in combining SEM-EDS and Raman spectroscopy for acquiring interconnected data is established in numerous publications in a large range of applications. A combination of SEM-EDS and Raman is frequently required in material sciences: SEM is a unique tool for imaging samples for morphological, chemical, and structural description, EDS provides the elemental composition, Raman spectroscopy provides structural information on minerals, such as polymorphism, the presence of chemical species (hydroxides, carbonates, organic compounds, fluid inclusions, etc.).

Theix *et al.* [25] combined SEM-EDS and Raman spectroscopy to identify and elucidate the structure of frapontite, a clay mineral. SEM and EDS are applied to the compositional analysis of the sample, identification of trace elements and purity of the sample (i.e., presence of unexpected phases). Aspects of the molecular structure are obtained by the band assignment of infrared (IR) and Raman spectroscopy. The frapontite "fingerprint" is obtained from the description of the Raman spectrum. Bruni *et al.* [26] combined SEM-EDS and vibrational spectroscopy (Raman and IR) for analysing blue pigments in polychrome artworks. Combining these techniques established the presence of several minerals such as lazurite, nosean, haüyne, and sodalite or their mixtures, which all are constituent parts of the rock mineral lapis-lazuli. They suggest their method enables to gain a complete and unambiguous characterisation of the colouring matter. Trace element zoning and incipient metamictisation in a lunar zircon were studied by Wopenka *et al.* [27], by combining secondary ion mass spectrometry (SIMS), electron probe microanalysis (EPMA), and Raman. Major and minor element concentrations were obtained from a thin section of zircon, by EPMA analysis. Trace element analyses were identified in situ with a SIMS. Raman spectroscopy is applied to study the changes in the crystalline structure of zircon caused by the decay of uranium, and thorium naturally presents in zircons. Raman spectroscopy can also be combined with other SEM-based techniques, like cathodoluminescence (CL) or electron backscatter diffraction (EBSD). Ishihara *et al.* [28] studied the epitaxial growth of graphene on a copper single crystal, to evidence the interest of Cu (111) for graphene synthesis. For this, the crystallographic orientation of the Cu surface is examined by EBSD before graphene synthesis by chemical vapour deposition (CVD). Raman map of the 2D to G peak ratio provides a direct determination of single-layer graphene (SLG) or few-layer graphene (FLG) growth. Zhu *et al.* [29] studied the influence of Nd^{3+}- and Yb^{3+}-dopants on the spectroscopic behaviour of Y_2O_3 ceramic by Raman and CL. Lattice distortion induced by the dopant incorporation and variations of effective absorption coefficients by adding different dopants were assessed using Raman, while the sample homogeneity is evidenced by the local intensity of CL bands. SEM-EDS and Raman spectroscopy were used by Tribaudino *et al.* [30] to explore and understand the mineralogy and texture of an altered Ca-Al-rich inclusion in a carbonaceous chondrite.

The analytical problems presented by the combined use of these two separate devices is evident according to these examples. Several authors also noticed the limitations of coupling data from these techniques on separate devices. These can be due to optical microscopy limitations (resolution, depth of field), and difficulties in locating particles of a few tens of µm from one device to the other. These analytical problems may lead to inconsistencies between data from the two techniques. Figure 3 presents the same area observed by light microscopy and SEM to identify observable amphibole particles/fibres. It can be complex to find an area of a few hundred µm on a sample of several cm, with significant differences in visualisation. Moreover, many fibres are visible by light microscopy (LM), whereas they are much less numerous on the backscattered electron (BSE) image. This, therefore, means that many fibres are included in the mineral matrix, and they do not emerge at the surface of the sample. These visualisation differences can lead to misidentification or misinterpretation in the combination of

data. The combined use of SEM-EDS and Raman is relevant to characterise these fibres, but the co-location of analyses appears difficult and time-consuming. Several authors have proposed technical solutions to address the problem of particle location. One of the solutions is the use of TEM reference grids or centre-marked grids on a SEM stub as particle support [31-34]. This solution is well suited to micrometre particles, the size of which ranges from several micrometre to several tens of micrometre and in all cases less than the length of the side of the grid holes (54 µm for a 300 mesh grid) and with a unique and homogeneous composition. However, the problem remains for larger particles (no ‘‘large hole’’ referenced grids), for nanometre particles (too small for LM), or for heterogeneous particles (which is the case for crushed rock for example). Another problem lies in the transport of such a sample from SEM to Raman [35]. Another problematic aspect is related to the depth of field of SEM compared to LM. Thus, particles with strong topography can be easily identified in the SEM but not with LM. Finally, it is important to note that the SEM image is formed from electron-material interactions localised in a thickness of a few nm (SEM) to a few µm (EDS), while the LM can provide details lying several µm, or even several mm below the surface. Thus, errors can be made in the location of the analysed point.

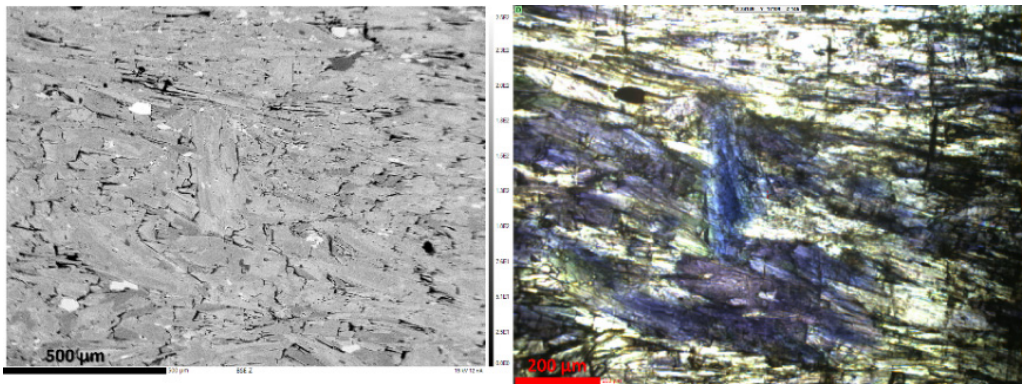

Figure 3. BSE (left) and light microscopy (right) images of a rock sample. Basic intercalation in glaucophane bearing basic rock (North Corsica, France).

2.2. A short history

Although both techniques have followed a parallel but different evolution since their introduction in the early 1930s, the concept of Raman-in-SEM coupling first began in the 1980s. SEM and µ-Raman appear to be essential for the characterisation of the morphology and the elemental and structural chemical properties of materials and minerals. Each technique provides complementary information that can be obtained at the micrometre scale. The data provided by each technique on its own is frequently insufficient in itself and has to be combined with data from the other technique. Moreover, compared to optical microscopy, SEM imaging offers a wide range of well-adapted contrasts for distinguishing regions of interest through their chemistry, morphology, crystallography, etc. Their coupling in a unique tool provides a promising analytical combination for such studies.

In the 1980s, Truchet and Delhaye proposed and patented a description of an optical system for simultaneous μ-Raman, electron microscopy imaging, and WDS elemental analysis in an electron microprobe (EPMA) or a transmission electron microscope (TEM) [36-38] (Fig. 4). They discussed the technical 'state of the art' and the potential interest in biology [39]. EPMA was chosen instead of SEM because of the optical microscope (Cassegrain-type optics) with a micrometre depth of field, placed in the objective lens of the electron optics. They modified the optical system by adding a special device equipped with a semi-transparent plate for sending a laser beam onto the sample surface and transmitting scattered light to the spectrometer. A major obstacle was the very low numerical aperture of Cassegrain objectives, thereby limiting the application field of such Raman spectroscopes to high-scattering samples.

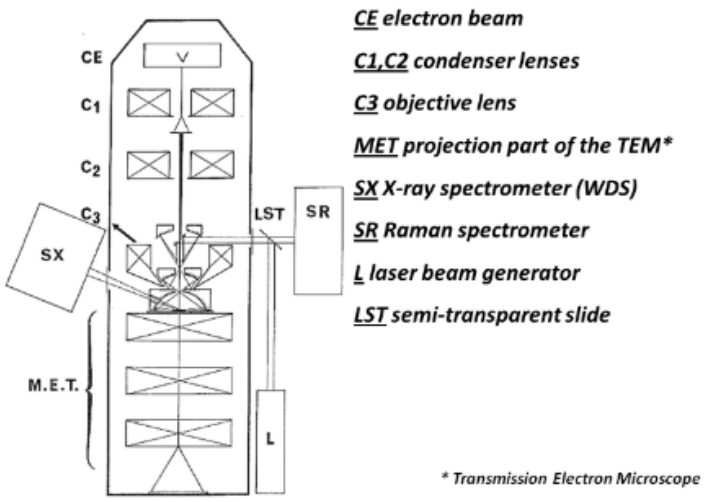

Figure 4. Schematic section of the EPMA column equipped with the Raman microprobe device (after [37]).

2.3. Integrated solutions for coupling SEM-EDS and Raman microscopy

Following the first developments, the first commercial systems were marketed in the early 2000s. To date, two technical coupling configurations are available on the market [40, 41] (Fig. 5).

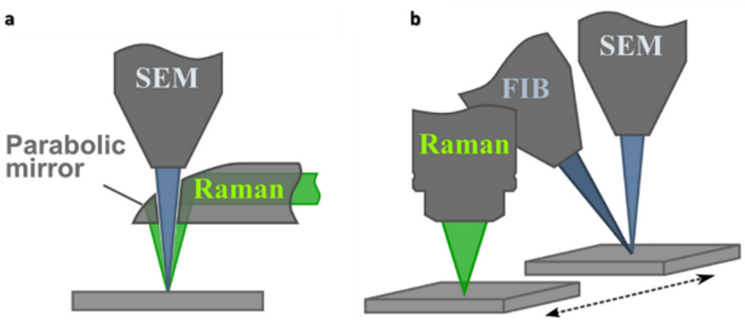

Figure 5. Different SEM - Raman setup: a) coaxial setup b) parallel setup (after [41]).

2.3.1. Co-axial setup. The first technical solution consists of a special interface comprising a parabolic mirror specifically developed for Raman spectroscopy (Figs. 5a to 5c) or a cathodoluminescence mirror (Fig. 5d) connected to a spectrometer. The mirror is placed on an automated retractable arm (Fig. 5a). This system is designed for precisely inserting and retracting the mirror under the pole piece of the SEM, between the SEM electron optics and the sample. An aperture in the mirror allows the electron beam to pass through. The laser radiation is focussed on the sample surface by the mirror. In this case, SEM and Raman use are independent. In the first version of this system, the mirror was fixed and allowed only spot acquisition of Raman spectra (Figs. 5a and 5b). Recently, new developments have been marketed, with a mobile mirror (3 axes), to acquire 2D and 3D data (Fig. 5c). An optical image is collected by the system, making it possible to precisely locate the laser spot on the sample. This image can also be used to check the good agreement between the SEM image and laser beam location. The system enables the collection of a large field-of-view optical image (up to 2 mm × 2 mm) for image correlation. This interface is connected to a conventional micro-Raman spectrometer using optic fibres.

The main interest of such a co-axial system is the ability to collect SEM-EDS and Raman data without moving the sample. However, it is necessary to retract the mirror for acquisition like BSE images (the mirror is positioned under the SEM pole piece) or EDS (the EDS detector is masked by the mirror). Some examples of a co-axial setup are shown in Fig. 6.

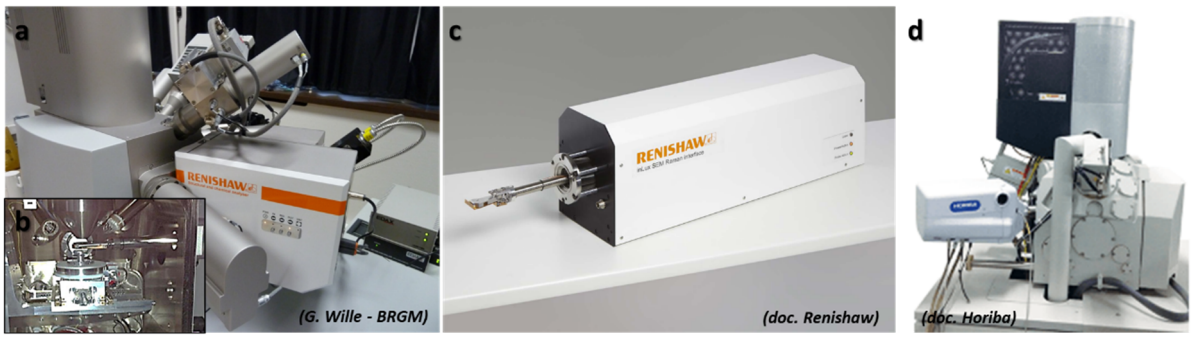

Figure 6. Examples of co-axial setup/ a) and b) Raman-in-SEM facility at BRGM (Orleans, France): Renishaw SEMSCA interfaced on a TESCAN MIRA 3 XMU and mirror in analysis position; c) Renishaw InLux system; d) Horiba RCLUE.

2.3.2. Parallel setup. In the parallel setup, the Raman microscope objective is placed some distance away parallel to the electron column (Fig. 5b). The SEM stage is then used for precisely repositioning the sample between Raman and SEM optics. The primary advantage is that the user benefits from the capabilities and performance of a confocal Raman microscope, particularly in terms of resolution, confocality, and signal intensity without affecting the performance of the SEM itself. Some examples of a parallel setup are shown in Fig. 7.

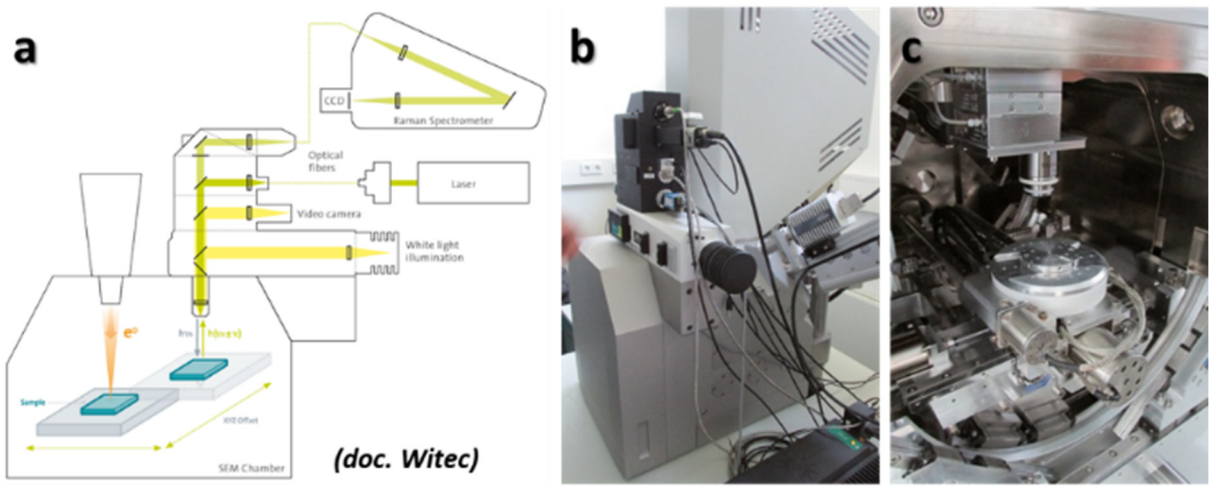

Figure 7. Examples of parallel setup: a) Schematic diagram of the Witec RISE system; b) and c) Witec RISE interfaced on a TESCAN MIRA and interior view of the SEM chamber.

2.4. Which SEM for coupling with Raman spectroscopy

Due to the electron negative charge, SEM samples have to be conductive or coated. To be Raman active, the sample must have vibrations (or rotations) that result in a change in the polarisability of the molecule or material. Since metals are (in first approximation) infinitely polarisable, a vibration of the atoms in the crystal lattice could not cause a change in the polarisability. In the case of metal, Raman diffusion can only be observed for the surface layer (oxidation, contamination), precipitates in alloys (carbides, borides…),… In the case of non-conductive samples, the accumulation of electronic charges at the point of impact of the beam is known to generate charging effects, which is detrimental to observation and analysis. To avoid having a charge built-up on the surface of non-conductive samples, the surface is usually coated with a conductive layer. When performing EDS analysis, carbon coating is usually recommended. However, carbon coating causes artefacts on the Raman spectrum, which can strongly affect its quality and subsequent data interpretation: a broad band can be observed around 1,500 cm^{-1} and the baseline level is much higher on the coated sample than on the same non-coated sample (Fig. 8). The bands are related to the carbon layer: The Raman spectrum of the amorphous carbon layer is characterised by a broad Raman band observed in the range of 1,000 - 1,800 cm^{-1} and this band can be well fitted by two Gaussian distributions known as “D” and “G” bands (band positions: 1,350 and 1,530 cm^{-1} for Scheibe *et al.* [42] or 1,380 and 1,560 cm^{-1} for Marchon *et al.* [43]). The baseline modification is due to the fluorescence phenomenon. The carbon coating behaves as a fluorophore (a compound that causes a molecule to absorb energy at a specific wavelength and then re-remit energy at a different wavelength). Moreover, the presence of the amorphous carbon layer produces a loss of Raman signal intensity and artefacts (fluorescence), as shown in Fig. 8 [44]. Under these conditions, the use of a conventional SEM is problematic. Capacities offered by recent FE-SEMs provide good quality images even at low

voltage (< a few kV) and make it possible to observe non-coated non-conductive samples in the SEM, but then, EDS microanalysis is difficult or even impossible. Then the use of a low vacuum (or environmental) SEM can be considered the most relevant solution Raman in SEM.

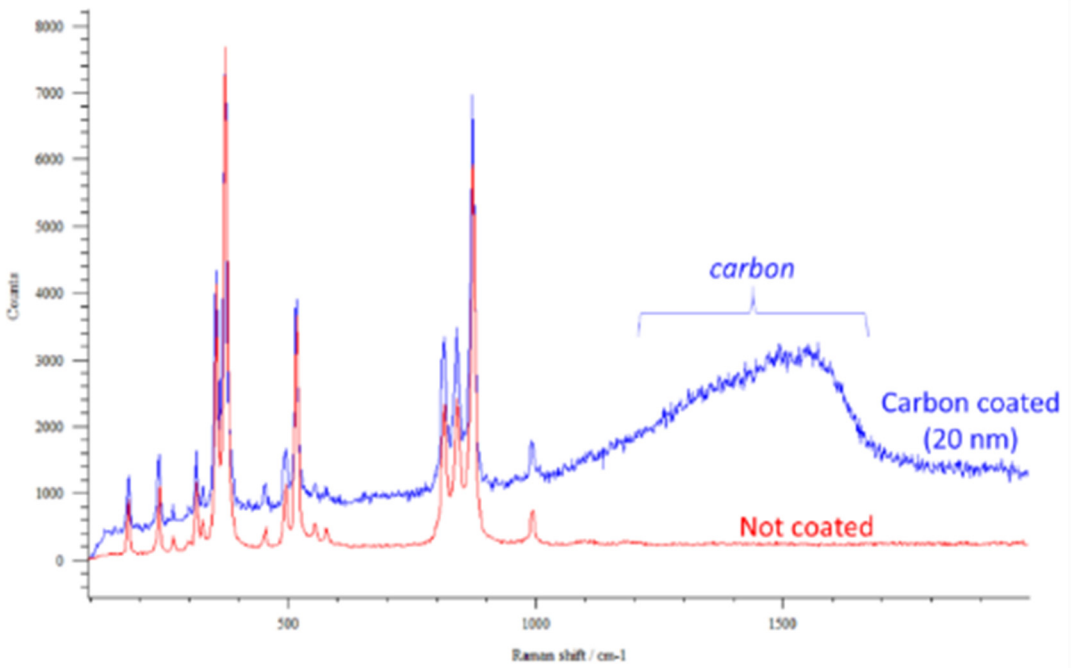

Figure 8. Effect of the carbon coating on the Raman spectrum of an Andradite grain (after [44]).

2.5. Cross-influence of the combined use of SEM and Raman

Coupling techniques may cause artefacts directly related to the influence of one on the other. Since Raman-in-SEM spectroscopy can be subject to several influences due to SEM, some possible artefacts, which are due to the impact of the electron beam, can be noticed on the Raman spectra [40, 44].

2.5.1. Contamination. Electron beam-induced contamination has been a well-known problem since the beginning of electron microscopy. It results from the development of carbon deposition on the scanning area. Different sources of contamination have been highlighted and discussed as well as methods to reduce contamination sources and consequences [45]. Since contamination leads to the growth of a thin layer of amorphous carbon on the sample surface, the expected effects are the same as those obtained by conductive carbon layer deposition. An example is shown in Fig. 9: A Raman spectrum is collected on cassiterite (SnO_2) after EDS mapping. A broad band is observed at the amorphous carbon bands positions [44]. Its intensity is affected by SEM parameters that influence the development of the contamination layer, like the duration of the electron beam scan, the beam parameters (HV, beam current), etc.

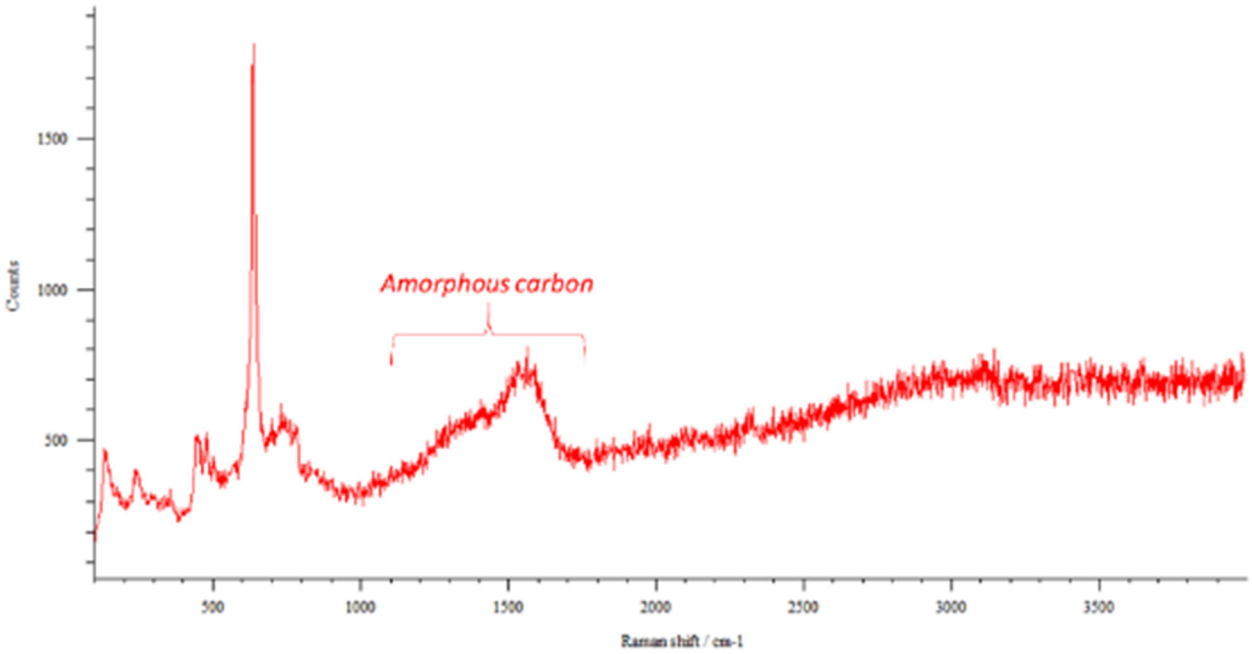

Figure 9. Contamination layer on a cassiterite sample after EDS map collection (after [44]).

2.5.2. Cathodoluminescence. Cathodoluminescence (CL) is a photonic emission phenomenon observed when an electron beam (in an SEM, for example) interacts with a sample. CL has many applications in various fields, for example, semiconductors, archaeo-materials, jewellery, mineralogy, and even biological or pharmaceutical samples. CL emission occurs in the visible / near-visible wavelength range, i.e., in the same range as Raman spectroscopy. Therefore, CL can generate artefacts in Raman spectra if not controlled and taken into account. Simultaneous use of both Raman spectroscopy and SEM scanning on a luminescent material causes the appearance of CL bands that are superimposed on the Raman scattering signal [44] as shown in Fig. 10.

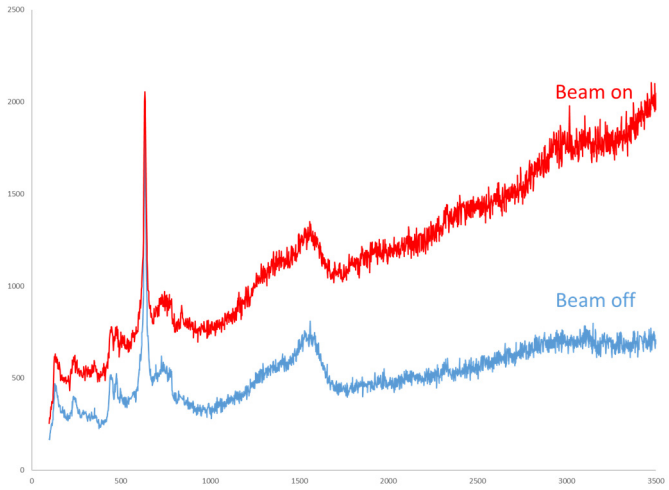

Figure 10. Raman spectrum of cassiterite with (red) and without (blue) electron beam (after [44]).

3. *RAMAN IN SEM: APPLICATIONS*

3.1. On-axis setup application on Alabaster microstructure of medieval statuettes

Alabaster is a soft rock, often used for carving. Chemically, alabaster is made of fine-grained gypsum, a hydrous sulphate of calcium. Another rock alternatively named "Egyptian alabaster", and "Oriental alabaster", is made of calcite, a carbonate of calcium. Raman spectroscopy is one of the techniques that can distinguish alabaster from Egyptian alabaster. The purest alabaster is a snow-white material, often associated with other mineral grains (silicates, carbonates, iron oxides), which produces brown clouding and veining in the stone. The softness of alabaster enables it to be carved readily into elaborate forms, but its solubility in water renders it unsuitable for outdoor work. Knowledge of the origin of the alabaster helps to understand the trade routes of this natural material, and isotopic techniques help provide a fingerprint of the different sources of supply [46]. Alabaster is generally veined with white and coloured veins. The objective of the study was the description the microstructure and the mineralogy of these veins, to understand their nature and composition. A slice of an alabaster sample was cut and polished. White and coloured veins are visible. Some of these veins were marked so that they can be identified in the SEM (Fig. 11a). The veins were investigated by SEM-EDS (Fig. 11).

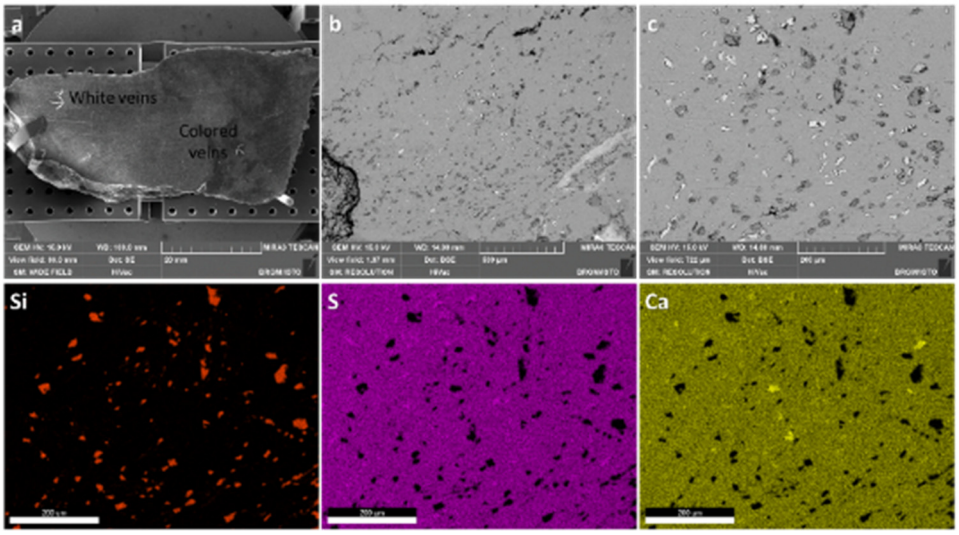

Figure 11. a) SEM (BSE) images of the sample, and b and c) details on a coloured veins. Lower row: EDS mapping (silicium – Si, sulphur – S, calcium – Ca).

The BSE images on the coloured veins highlight different grains of various compositions. The microstructure shows the presence of different minerals that are easily identified by EDS as quartz (SiO_2) and various silicates, as well as calcium carbonates. The map of sulphur shows the presence of grains of calcium sulphate, slightly different from the matrix composed of gypsum

These sulphate grains are also present in the white veins. In these veins, we can also note the presence of clear grains on the BSE image, corresponding to celestine ($SrSO_4$) (Fig. 12). The abnormal sulphate grains show similar EDS analysis, and the completion of quantitative analyses is made difficult by the presence of significant porosity of the materials. Further investigations are needed and Raman spectroscopy is a relevant technique for identifying the constituent mineral of these grains. However, optical microscopy does not make it possible to easily differentiate the different grains. Therefore, the use of a suitable visualisation mode such as BSE in the SEM is required. The Raman spectra of gypsum and abnormal sulphate grains are, therefore, collected in the SEM using a Renishaw SEMSca coupled to an InVia spectroscope (Fig. 6a). Operation conditions were: wavelength 514 nm, power 25 mW, collection duration 200 sec (spectrum accumulation mode).

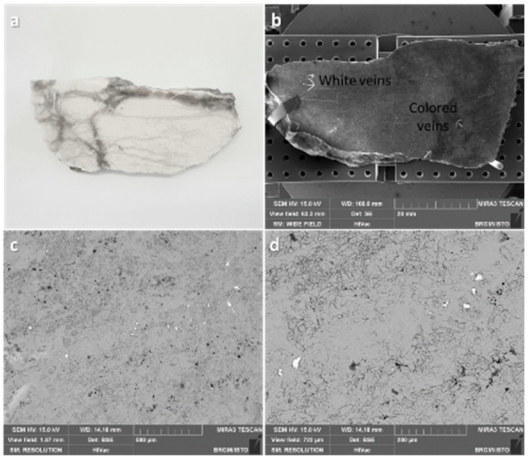

Figure 12. Alabaster sample: a) photography, and b) SEM-BSE; c and d) details on a white vein showing celestine grains (BSE: clear grains).

The comparison of the spectra is presented in Fig. 13. The mineralogical identification of abnormal phases was performed by searching in a database (RRUFF Database [47] - R040061 record) and confirmed by the bibliographic data [48, 49]. The grains are identified as anhydrite, an anhydrous calcium sulphate. The anhydrous character of the calcium sulphate is highlighted by the absence of Raman bands around 3,500 cm^{-1} (-OH stretching vibration).

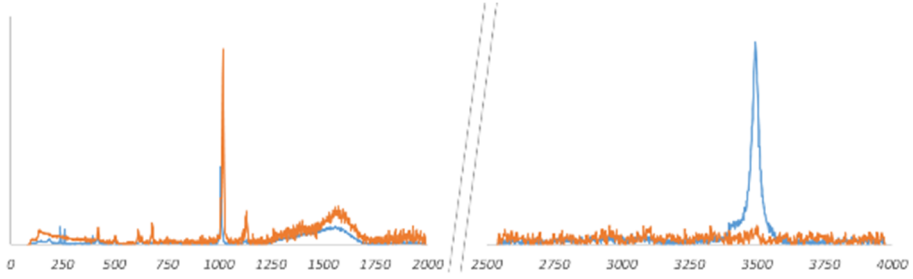

Gypsum	Anhydrite
185	
236	
259	
393	
417	419
494	499
621	612
	629
	679
1010	1019
	1130
3494	

Figure 13. Raman spectra of gypsum (blue) and abnormal sulphate grain (orange) - detected Raman bands position (Raman shift, in cm^{-1}).

3.2. Parallel setup application of high-resolution 2D and 3D imaging on naturally occurring asbestos

Asbestos is a term describing six fibrous silicate minerals that form bundles of long and thin mineral fibres (sub-micrometre diameter). The form and structure of these fibres are called asbestiform. The term asbestos initially refers to minerals marketed and used industrially and, in countries that have regulated or prohibited their use, it is defined by regulation (for example, in Europe, the directive 99/77/EC). The term asbestos usually refers to one fibrous serpentine (chrysotile), and five asbestiform varieties of amphiboles: asbestiform varieties of riebeckite (crocidolite), anthophyllite (anthophyllite-asbestos), grunerite (amosite), actinolite (actinolite-asbestos), and tremolite (tremolite-asbestos) [50, 51], even if other minerals can crystallise in a similar habit [52]. If these materials have been (and still are) used industrially, they are initially obtained by extraction in mines, i.e., asbestos initially results from a natural process. Then the term "naturally occurring asbestos" (NOA) refers to fibrous minerals that are found in certain rocks or soil as a result of natural geological processes. Examples of NOA are presented in Fig. 14. Natural weathering and routine human activities may disturb NOA-bearing rock or soil and release mineral fibres into the air, which pose a potential risk for human exposure by inhalation. A large set of metamorphic rocks may contain asbestos fibres (meta-ophiolitic rocks of basic or ultrabasic compositions [53-55], hydrothermally altered dolerites [56], talc deposits [57], metamorphosed dolostones and iron formations [58] or sub-alkaline plutonic rocks [59]. Asbestos is considered a Category 1 human carcinogen [51, 53, 54, 60, 61], as inhalation of asbestos fibres causes respiratory diseases, in particular asbestosis, lung cancers, and malignant mesothelioma.

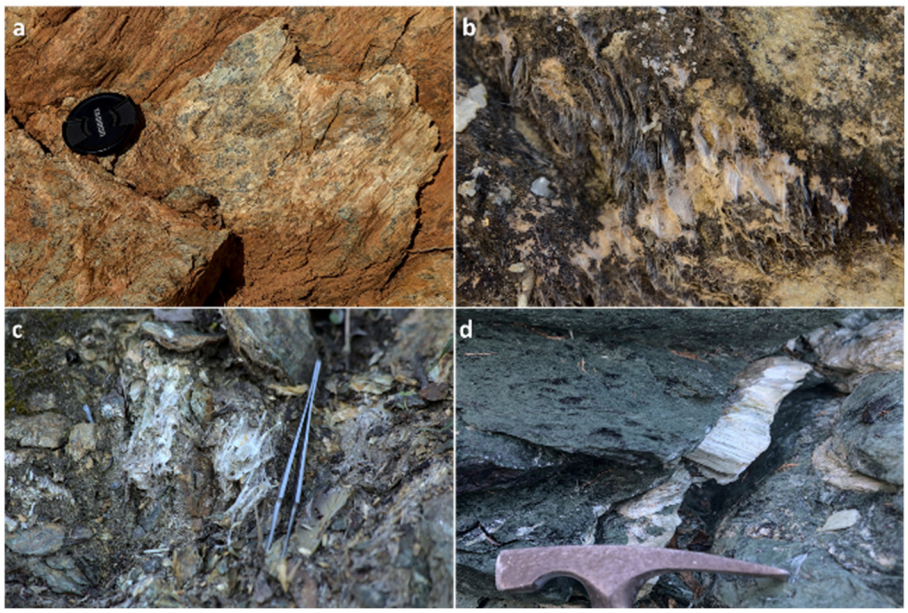

Figure 14. Examples of naturally occurring asbestos: a) "slip-vein" with chrysotile cutting serpentinites; b) polymineral vein with actinolite-asbestos cutting ophiolitic metagabbro; c) clusters of tremolite-asbestos fibres in mylonitic and d) cataclastic serpentine.

Optical microscopy is the most currently used method for the regular measuring of asbestos, although it does not allow identification and counting of individual fibres detrimental to health [62]. The transmission electron microscope (TEM) is the most efficient method for asbestos diagnosis in air, due to its capacity to provide morphology, chemistry, and crystallographic information together on the same fibre [63]. But in the case of amphibole included in a mineral matrix, TEM is hard to apply: it is likely to release artefacts like cleavage fragments due to sample crushing, and sample-piece thinning by ion beams techniques is costly and hard to achieve and thus not applicable in routine analysis. In addition, the differentiation of real asbestos fibres and cleavage fragments of non-asbestos amphiboles (created by a grinding step in the protocol) is complex in many cases and the criteria proposed by different authors, if they are often relevant, are not completely discriminating [64-66] and can lead to "false positive" result. In addition, it can also be questioned about the representativeness of the sampling of some cubic micrometres compared to the heterogeneity of a sample at the scale of several millimetres or even centimetres. Then the development of an alternative analysis protocol, adapted in terms of spatial resolution and mineralogical discrimination capabilities, and which does not generate sample preparation artefacts, is relevant.

Among the methods that meet these criteria, the combined use of SEM-EDS and Raman spectroscopy is a relevant solution [67, 68]. Indeed, the resolution of SEM imaging makes it possible to easily observe fibres of less than a few hundred nm in diameter. Combined with EDS analysis, Raman spectroscopy can provide a mineralogical signature of the serpentine [69-71] or amphibole [72, 73]. But, above all, these techniques, combined within the same analytical system, can be applied to a coherent rock sample (polished section or thin geological section), without prior grinding (therefore, without generating cleavage fragments linked to the sample preparation [65, 74-77]). Confocal Raman-in-SEM can be performed on any polished SEM sample. Samples were prepared as thin geological slices: A block of rock is glued on a glass slice then thinned and polished to a thickness of 40 µm. The samples were observed by polarized light microscopy (PLM) before SEM analysis, for a petrographic study and location of regions of interest (i.e., presence of fibrous / non-fibrous amphiboles). The nature of amphiboles was confirmed by EPMA analyses on the micrometre particles/bundles. Coupled SEM observations and Raman imaging in SEM were performed on a TESCAN-Witec RISE microscope combining a TESCAN Mira 3 GMU LV-FE-SEM coupled to a WITec confocal Raman imaging system. The RISE confocal Raman imaging system is equipped with a UHTS300 spectrometer, a Zeiss 100x vacuum objective (numerical aperture N.A. = 0.75) mounted inside the SEM chamber, using a 532 nm laser radiation wavelength. Coupled SEM-EDS and Raman imaging was performed on non-coated samples at HV = 15 kV under low vacuum conditions (nitrogen, pressure 20 - 40 Pa).

An example is presented in Fig. 15. A thin geological slice was prepared on a rock from a stone quarry. EPMA analyses prove the presence of actinolite does not make it possible to precisely identify the nature of the thinnest particles with a diameter of less than 1 µm. Confocal Raman is collected in the SEM: The thinnest fibres are located using the SEM imaging and EDS analysis

(Figs. 15a and 15b), then a Raman map is collected on the same area light microscopy image is first collected (Fig. 15c) the Raman mapping is performed on a selected area. After data analysis, the spectra of the two phases present are identified by analysis of the data cube, allowing the production of a phase map and the corresponding spectra (Figs. 15d and 15e). The confocal Raman mapping makes it possible to identify actinolite fibres in an orthoclase matrix, including the thinnest fibres, with a diameter of 400 nm or less.

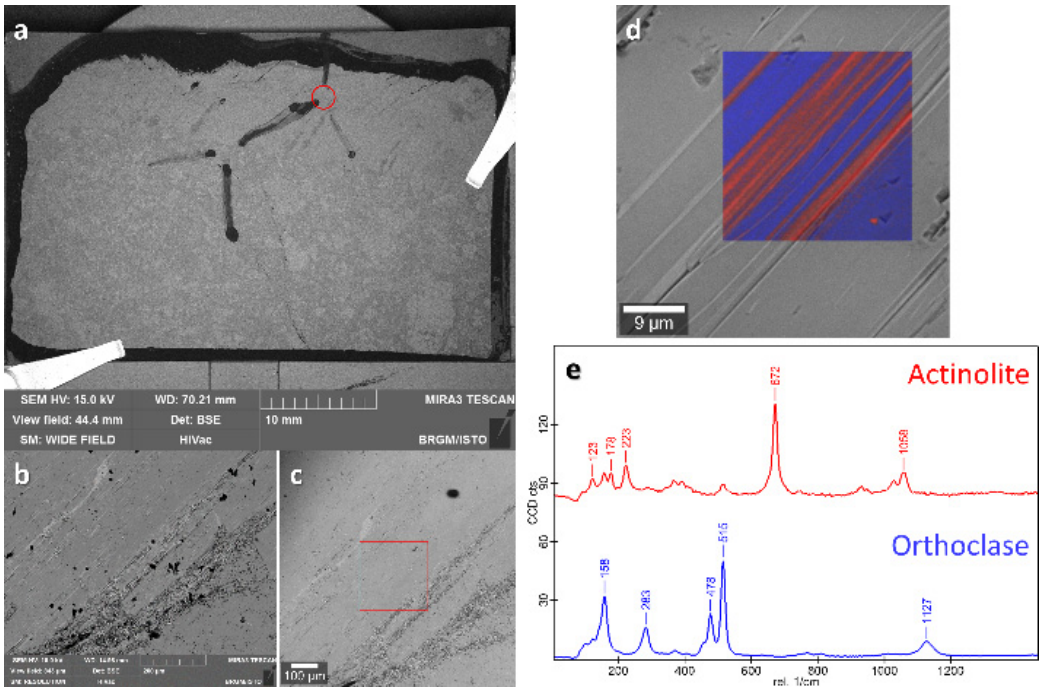

Figure 15. Confocal Raman-in-SEM analysis of actinolite fibres in an orthoclase matrix (south of the Armorican Massif, France).

A confocal microscope is a system for which illumination and detection are limited to the same volume of reduced size. The resolution is directly related to the value of the numerical aperture (N.A.). When the system is highly confocal, it allows a short resolution in Z. If the material is transparent to the laser radiation, the confocal Raman-in-SEM also allows the acquisition of 3D measurements by combining a series of maps along the Z axis. An example is presented in Fig. 16. A series of maps are collected with a step of 0.5 µm from the surface to 20 µm then combined to produce a 3D volume. In Fig. 16a, a 2D map is presented. Actinolite particles or fibres are visible on the surface. The interest of the 3D view is to provide information on the true shape of the particles of actinolite in the matrix and to make it possible to determine a volumetric quantity of fibres, a data very difficult to establish due to the nanometre dimension of the fibres. For example, on the 3D map, a short elongated particle of actinolite on the 2D map (circle) is detected. Using the 3D view, it is possible to identify this particle as being in fact, a fibre positioned obliquely to the surface of the sample.

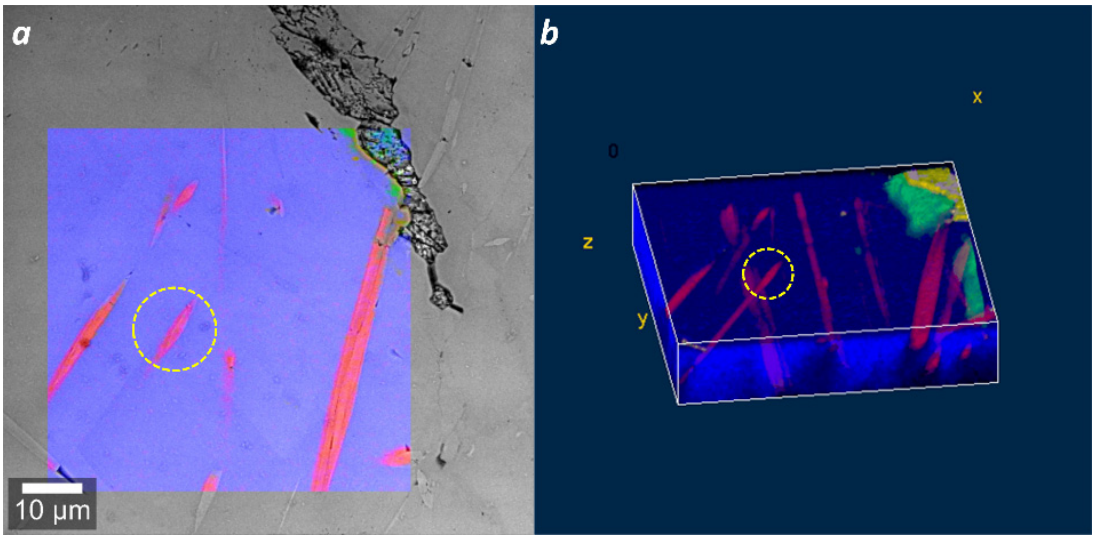

Figure 16. 3D Raman-in-SEM: actinolite fibres (red) in albite (blue) (after [66]).

4. CONCLUSION

The interest in combining SEM-EDS and Raman spectroscopy for the characterisation of materials is highlighted by numerous authors for many years. The emergence of devices that integrate these two techniques in a single analytical system has revealed new capabilities for co-located data correlation. Raman-in-SEM is a powerful combination of two mature technologies, which results in a set of chemical and structural data that redefine convenience, efficiency, and productivity in the characterisation of materials. Numerous applications are mentioned in the literature, including materials sciences, industrial processing, nanotechnologies, corrosion or oxidation of reactive phases, multilayer deposits, life sciences, etc. In geosciences, the combination of elemental and crystallographic analysis is frequently required to identify and describe a mineral. Mineralogical analysis requires a set of analytical imaging techniques to access a thorough knowledge of the sample and better understand the mineralogical, chemical, and textural factors that control their behaviour and reactivity. Among these techniques, SEM and µ-Raman spectroscopy occupy a major place among the characterisation techniques. SEM provides various information on morphology, topography, and chemistry at a nanometre scale, supplemented by elemental and crystallographic analysis. Raman spectrum is a sort of fingerprint of a given compound and the technique is sensitive to various elements of the local environment. It can reveal a mineral's crystal structure, providing details on its chemical and structural properties. Raman offers various information that includes, among others, the identification of polymorphs, crystallographic orientation, evaluation of temperature, and stress effects on the structure. Moreover, Raman provides complementary chemical and structural information to that obtained from SEM. This is why both are often used in parallel. Then, coupling SEM-EDS and Raman spectroscopy and imaging on the same analytical system appears to be an efficient method of identifying the mineral nature and

determining the structural properties of geomaterials. This multi-technique microscopy allows the collection of a real mineralogical analysis of rocks. This coupling makes it possible to solve problems for the diagnosis and the mineralogical characterisation of geomaterials.

5. REFERENCES

[1] Brillouin L 1922 *Ann. Phys. (Paris)* **9** 88-122
[2] Smekal A 1923 *Naturwissenschaften* **11** 873-875
[3] Raman C V, *et al.* 1928 *Nature* **121** 501-502
[4] Lord Rayleigh 1881 *London, Edinburgh, Dublin Philos. Mag. J. Sci.* **12** 81-101
[5] Begliarbekov M, *et al.* 2010 *Appl. Phys. Lett.* **97** 031908
[6] Fischer S, *et al.* 2011 *Fusion Sci. Technol.* **60** 925-930
[7] Jamur J 2022 *Spectrosc. Eur.* **34** 18-22
[8] Angel R J, *et al.* 2019 *Zeitschrift Für Krist. - Cryst. Mater.* **234** 129-140
[9] Ma L, *et al.* 2021 *Microelectron. Reliab.* **118** 114045
[10] Liu D, *et al.* 2014 in: *Spectroscopic properties of inorganic and organometallic compounds*. (Douthwaite R, Duckett S and Yarwood J (Eds.)) [London, United Kingdom: Royal Society of Chemistry] Tech. Mater. Appl. 45 141-177
[11] Tan P-H 2019 Raman spectroscopy of two-dimensional materials. [Singapore: Springer]
[12] Cong X, *et al.* 2020 *npj 2D Mater. Appl.* **4** 13
[13] Taghizadeh A, *et al.* 2020 *Nat. Commun.* **11** 3011
[14] Malard L M, *et al.* 2021 *Phys. Chem. Chem. Phys.* **23** 23428-23444
[15] Casadio F, *et al.* 2016 *Top. Curr. Chem.* **374** 62
[16] Lofrumento C, *et al.* 2004 *J. Raman Spectrosc.* **35** 650-655
[17] Gueriau P, *et al.* 2017 *Anal. Chem.* **89** 10819-10826
[18] Colomban P 2004 *Appl. Phys. A* **79** 167-170
[19] Armbruster T, *et al.* 2016 Highlights in mineralogical crystallography. [Berlin, Germany: De Gruyter]
[20] Hope G A, *et al.* 2001 *Miner. Eng.* **14** 1565-1577
[21] Griffith W P 1969 *Nature* **224** 264-266
[22] Frezzotti M L, *et al.* 2012 *J. Geochemical Explor.* **112** 1-20
[23] Caumon M, *et al.* 2020 *J. Raman Spectrosc.* **51** 1868-1873
[24] Beyssac O, *et al.* 2002 *J. Metamorph. Geol.* **20** 859-871
[25] Theiss F L, *et al.* 2015 *Spectrochim. Acta A: Mol. Biomol. Spectrosc.* **147** 230-234
[26] Bruni S, *et al.* 1999 *Vibr. Spectrosc.* **20** 15-25
[27] Wopenka B, *et al.* 1996 *Am. Mineralogist* **81** 902-912
[28] Ishihara M, *et al.* 2011 *Mater. Lett.* **65** 2864-2867
[29] Zhu W, *et al.* 2013 *J. Phys. Chem. A* **117** 3599-3607
[30] Tribaudino M, *et al.* 2021 *J. Raman Spectrosc.* **52** 1892-1901
[31] Stefaniak E A, *et al.* 2006 *Spectrochim. Acta B: Atom. Spectrosc.* **61** 824-830
[32] Stefaniak E A, *et al.* 2009 *J. Hazard. Mater.* **168** 416-423

[33] Pointurier F, *et al.* 2010 *Spectrochim. Acta B: Atom. Spectrosc.* **65** 797-804
[34] Godoi R H M, *et al.* 2006 *Spectrochim. Acta B: Atom. Spectrosc.* **61** 375-388
[35] Nelson M P, *et al.* 2001 *Aerosol Sci. Technol.* **34** 108-117
[36] Truchet M, *et al.* 1986 *Dispositif de microscopie analytique propre à former à la fois une sonde Raman et une sonde électronique*. Patent FR2596863A1
[37] Truchet M, *et al.* 1988 *J. Microsc. Spectrosc. Electron.* **13** 167-197
[38] Dhamelincourt P, *et al.* 1991 *J. Raman Spectrosc.* **22** 61-64
[39] Truchet M, *et al.* 1988 *Biol. Cell* **63** 26
[40] Wille G, *et al.* 2014 in: *Spectroscopic properties of inorganic and organometallic compounds*. (Douthwaite R, Duckett S and Yarwood J (Eds.)) [London, United Kingdom: Royal Society of Chemistry] Tech. Mater. Appl. 45 79-116
[41] Jiruše J, *et al.* 2014 *J. Vac. Sci. Technol. B: Nanotechnol. Microelectron. Mater. Process. Meas. Phenom.* **32** 06FC03
[42] Scheibe H-J, *et al.* 1995 *Fresenius. J. Anal. Chem.* **353** 695-697
[43] Marchon B, *et al.* 1997 *IEEE Trans. Magn.* **33** 3148-3150
[44] Wille G, *et al.* 2014 *Micron* **67** 50-64
[45] Postek M T 2006 *Scanning* **18** 269-274
[46] Kloppmann W, *et al.* 2017 *Proc. Natl. Acad. Sci.* **114** 11856-11860
[47] Lafuente B, *et al.* 2016 in: *Highlights in mineralogical crystallography*. [Berlin Germany: De Gruyter] 1-30
[48] Berenblut B J, *et al.* 1973 *Spectrochim. Acta Part A: Mol. Spectrosc.* **29** 29-36
[49] Berenblut B J, *et al.* 1971 *Spectrochim. Acta Part A: Mol. Spectrosc.* **27** 1849-1863
[50] WHO 1986 *Environmental health criteria 53: Asbestos and other natural mineral fibers*. [Geneva, Switzerland: World Health Organisation]
[51] Niosh 2011 *Curr. Intel. Bull.* **153**
[52] Lockey J 1981 *Clin. Chest Med.* **2** 203-218
[53] Vignaroli G, *et al.* 2014 Environ. Earth Sci. **72** 3679-3698
[54] Campopiano A, *et al.* 2018 *Int. J. Environ. Health Res.* **28** 134-146
[55] Lahondère D, *et al.* 2019 *Environ. Earth Sci.* **78** 540
[56] Lahondère D, *et al.* 2018 *Environ. Earth Sci.* **77** 385
[57] Van Gosen B S, *et al.* 2004 *Environ. Geol.* **45** 920-939
[58] Van Gosen B S 2007 *Environ. Eng. Geosci.* **13** 55-68
[59] Metcalf R V, *et al.* 2015 *Geology* **43** 63-66
[60] MSHA 2005 *Preliminary regulatory economic analysis for proposed rule on asbestos exposure limit*. [Washington DC: Department of Labor, Mine Safety and Health Administration]
[61] Lahondere D, *et al.* 2018 in: *Conf. Rep. XIII IAEG Congress*. (San Francisco, CA)
[62] Boulanger G, *et al.* 2014 *Environ. Health* **13** 59
[63] Steen D, *et al.* 1983 *Atmos. Environ.* **17** 2285-2297
[64] Van Orden D R, *et al.* 2008 *Indoor Built Environ.* **17** 58-68
[65] Belardi G, *et al.* 2018 *J. Mediterranean Earth Sci.* **10** 63-78
[66] Harper M, *et al.* 2008 *J. Occup. Environ. Hyg.* **5** 761-770

[67] Wille G, *et al.* 2018 *Microsc. Microanal.* **24** 2012-2013
[68] Wille G, *et al.* 2019 *J. Hazard. Mater.* **374** 447-458
[69] Groppo C, *et al.* 2006 *Eur. J. Mineral.* **18** 319-329
[70] Rinaudo C, *et al.* 2003 *Can. Mineralogist* **41** 883-890
[71] Petriglieri J R, *et al.* 2015 *J. Raman Spectrosc.* **46** 953-958
[72] Leissner L, *et al.* 2015 *Am. Mineralogist* **100** 2682-2694
[73] Bersani D, *et al.* 2019 *Minerals* **9** 491
[74] Langer A M, *et al.* 1987 *New Engl. J. Med.* **316** 882-882
[75] Bloise A, *et al.* 2018 *Minerals* **8** 274
[76] Baietto O, *et al.* 2019 *Fibers* **7** 52
[77] Militello G M, *et al.* 2020 Episodes **43** 909-918